Single-particle-like charge-density excitations in charged spherical semiconductor quantum dots

Chih-Li Weng and Yan-Chr Tsai*

Department of Physics, National Chung Cheng University, Chia-Yi 621, Taiwan
(Received 11 November 2008; published 24 June 2009)

The dynamic dielectric function of a spherical semiconductor quantum dot (QD) is derived analytically within the framework of the effective mass and Bohm-Pines' random-phase approximations. The computational schemes are developed to investigate the single-particle-like charge-density excitations (SP-like CDEs) in charged spherical QDs, which are observed in the resonant Raman scattering [C. Steinebach, C. Schüller, and D. Heitmann, Phys. Rev. B **59**, 10240 (1999)]. The formulism in this study is established in terms of the real-space representation, which is suitable for zero-dimensional systems. This study investigates the energy of the SP-like CDE with the angular quantum number l, and discusses the relation between this excitation and the single-particle excitation (SPE) energies. The selection rules of angular quantum numbers l play the important role in determining the SP-like CDE energies, and the calculated results are consistent with measurements. This study also presents the dependence of the energy shift in the SP-like CDE with respect to the SPE on the size of a QD. The calculated results imply that SP-like CDEs will disappear in the limit of a QD with an infinite large radius. The dependence of the energy shift on the relative permittivity ϵ_s is also discussed.

I. INTRODUCTION

In recent years, the elementary electronic excitation spectra of the semiconductor nanostructures have been studied with extensive efforts both experimentally and theoretically.[1–11] For instance, resonant Raman-scattering (RRS) technique[3,4,12–16] provides rich experimental spectra of these elementary electronic excitations in the nanostructures, such as single-particle excitations (SPEs), charge-density excitations (CDEs), and spin-density excitations (SDEs). As is known, excitation spectra depend crucially on the system dimensionality. Das Sarma and co-workers[1,3–5] derived the dynamic dielectric functions for the quasi-one-dimensional (Q1D) and two-dimensional (2D) graphene systems with dependence on frequency and wave number. The results were used to find the dispersion of the collective excitation mode and the electrostatic screening of the Coulomb interaction.[5] The linear-response theory[17] for the screening effect, tight-binding approximation (TBA), and Bohm-Pines' random-phase approximation (RPA) (Refs. 18 and 19) are major theoretical foundations.[7,8,11]

Moreover, Steinebach *et al.*[12–14] and Schüller[16] observed that, besides the strongly collective excitations, additional modes close to the SPE become resonant for certain laser energies in GaAs QDs. These additional modes display collective effects weakly.[12,16] These modes are subjected to a small energy shift with respect to the SPEs, and termed as single-particle-like (SP-like) modes.

In the present work, we specialize in the spherical QDs made of semiconductor materials, CdS, CdSe, and CdTe. The spatial confinement of carriers leads to some interesting physical properties of the zero-dimensional (0D) system, such as the energy shift in the SP-like CDE with respect to the SPE becomes measurable. Meanwhile, system dimensionality also brings about the difficulty in applying the earlier scheme developed for 2D and one-dimensional (1D) systems to 0D. The Lindhard dielectric function can be obtained for 2D and 1D systems, and the derivation can be found in

textbooks.[20,21] Through the Fourier transformation, one can deal with the problems in the momentum space for 2D and 1D systems, since both systems respect translational symmetry. In the 0D system, such as an isolated QD without translational symmetry, one must address the issue in terms of the real-space representation. We adopt the effective-mass approximation (EMA) (Refs. 22–24) to determine the electronic levels, and use the RPA to derive the dynamic dielectric function. Instead of using plane waves for expansion in 2D and 1D systems, the functions constructed by the carrier envelope functions serve as the appropriate expansion basis for the 0D system. Due to spherical symmetry of CdS, CdSe, and CdTe QDs, the angular dependence in the formulism is expressed in terms of spherical harmonics.

In this work, Sec. II analytically derives the electron dynamic dielectric function and the dielectric matrix elements. The single-band EMA is employed to obtain the electron envelope functions in a spherical QD. With the aid of the envelope functions, the RPA-based generalized polarization function is attained. Section II also expands the radial and angular parts of the Coulomb potential in terms of the spherical Bessel functions and spherical harmonics, respectively. Then, one can acquire the dielectric function and the dielectric matrix elements. Some details are presented in the Appendices. Section III numerically calculates the SP-like CDE energies by searching for zeros of the determinants for the dielectric matrix. The energy shift in the SP-like CDE with respect to the SPE is discussed. The Fermi level can be adjusted to control the number of occupied conduction states, i.e., the QD is charged or electron-doped. The dependence of the SP-like CDE energy on QD sizes of different materials is investigated, and the relation between the energy shift and the relative permittivity ϵ_s is also presented. Section IV summarizes our study and proposes the experiment, RRS, to probe the SP-like CDEs.

II. DYNAMIC DIELECTRIC FUNCTION

The expression for the dielectric function of a spherical quantum dot (QD) is derived analytically in this section. The

formulism is based on both the single-band EMA (Refs. 22–24) and RPA.[18,19,25,26] The former is employed to obtain the electron (or hole) envelope wave functions in a spherical QD, and the latter is adopted to determine the polarization function required to evaluate the dielectric function. We use spherical harmonics to expand the angular dependence in the formulism because of spherical symmetry in the systems.

The dynamic dielectric function $\epsilon(\mathbf{r}, \mathbf{r}'; \omega)$ is known to be expressed as[27–30]

$$\epsilon(\mathbf{r}, \mathbf{r}'; \omega) = \epsilon_s \delta(\mathbf{r} - \mathbf{r}') - \int d^3 \mathbf{r}'' v(\mathbf{r}, \mathbf{r}'') P(\mathbf{r}'', \mathbf{r}'; \omega), \quad (1)$$

where $\mathbf{r}$ and $\mathbf{r}'$ are position vectors, $\delta(\mathbf{r} - \mathbf{r}')$ is the usual Dirac delta function,[31] $v(\mathbf{r}, \mathbf{r}'')$ is the Coulomb interaction, and $P(\mathbf{r}'', \mathbf{r}'; \omega)$ denotes the polarization function. The dielectric constant ϵ_s is the permittivity of the semiconductor.[20] In this calculation, we treat $\epsilon_s \approx \epsilon(\infty)$ for different semiconductors, and $\epsilon(\infty)$ is the relative permittivity due to core and valence electrons.[20,32] The value of ϵ_s influences the Coulomb potential energy in semiconductors, which is relative to the strength of the screening effect, and will be discussed in Sec. III.

The essential feature of the calculation for the dielectric function is to expand $\epsilon(\mathbf{r}, \mathbf{r}'; \omega)$ by an appropriate complete set of wave functions such as

$$\epsilon(\mathbf{r}, \mathbf{r}'; \omega) = \sum_{ij} \Psi_i^*(\mathbf{r}) \epsilon_{ij}(\omega) \Psi_j(\mathbf{r}'), \quad (2)$$

and the same set of wave functions $\Psi_i(\mathbf{r})$ and $\Psi_j(\mathbf{r}')$ is used for expanding $v(\mathbf{r}, \mathbf{r}')$ and $\delta(\mathbf{r} - \mathbf{r}')$. The indices i and j denote the quantum numbers.

To obtain the appropriate complete set of wave functions, one should calculate the electronic structures in a spherical QD. According to the EMA, the stationary Schrödinger equation for the electron (hole) envelope function is known as[33]

$$\left[-\frac{\hbar^2}{2} \nabla \cdot \frac{1}{m^*} \nabla + V(\mathbf{r}) \right] \psi(\mathbf{r}) = E\psi(\mathbf{r}), \quad \text{where } V(\mathbf{r})$$
$$= \begin{cases} 0 & \text{if } r < R, \\ \infty & \text{otherwise,} \end{cases} \quad (3)$$

$\hbar$ Planck's constant divided by 2π, E the energy eigenvalue, $\psi(\mathbf{r})$ the corresponding eigenfunction, $\mathbf{r}$ the position vector, R the radius of the QD, and m^* the effective mass of the semiconductor material. Because of spherical (or isotropic) symmetry in the geometry of the QD, the confinement potential depends only on the radius r, i.e., $V(\mathbf{r}) = V(r)$, where $r = |\mathbf{r}|$. Then, the envelope function is written as the product of functions with radial and angular coordinates dependence:[22–24] $\psi_{lnm}(r, \theta, \phi) = N_{ln} j_l(k_{ln} r) Y_{lm}(\theta, \phi)$ $\equiv \Xi_{ln}(r) Y_{lm}(\theta, \phi)$, where $j_l(k_{ln} r)$ is the spherical Bessel function, $Y_{lm}(\theta, \phi)$ is the so-called spherical harmonics, N_{ln} is the corresponding normalized constant, and

$$k_{ln} = \sqrt{\frac{2m^* E_{ln}}{\hbar^2}}. \quad (4)$$

The infinite energy barrier between the vacuum and QDs will lead the wave function to vanish at $r = R$, which can determine k_{ln}. Here, the indices, l, n, and m, for the envelope function $\psi_{lnm}(r, \theta, \phi)$ are quantum numbers.

The polarization function will be calculated by neglecting the vertex correction in the Hedin equations[34,35] and using the expression of a noninteracting particle Green's function within the framework of RPA. With the previously obtained envelope function from EMA, the RPA-based generalized polarization function $P(\mathbf{r}, \mathbf{r}'; \omega)$ is attained as[27–29,36]

$$P(\mathbf{r}, \mathbf{r}'; \omega) = \sum_{l_1 m_1 n_1}^{\text{occ}} \sum_{l_2 m_2 n_2}^{\text{unocc}} \Xi_{l_1 n_1}^*(r) \Xi_{l_2 n_2}(r) \Xi_{l_2 n_2}^*(r') \Xi_{l_1 n_1}(r')$$
$$\times Y_{l_1 m_1}^*(\theta, \phi) Y_{l_2 m_2}(\theta, \phi) Y_{l_2 m_2}^*(\theta', \phi') Y_{l_1 m_1}(\theta', \phi')$$
$$\times \left\{ \frac{1}{\hbar\omega - E_{l_2 n_2} + E_{l_1 n_1} + i\eta} \right.$$
$$\left. - \frac{1}{\hbar\omega + E_{l_2 n_2} - E_{l_1 n_1} - i\eta} \right\}, \quad (5)$$

where η is the damping factor. In Eq. (5), the first summation stands for all occupied states, and the second one sums over all unoccupied states. Note that the spin of carriers is not considered in the calculations. Based on the EMA, the radial envelope functions are real, which implies that $\Xi^*(r) = \Xi(r)$.

Similarly, the Coulomb potential energy $v(\mathbf{r}, \mathbf{r}')$ should be expanded by the complete set of wave-functions $\Psi_i^*(\mathbf{r})$ and $\Psi_j(\mathbf{r})$

$$v(\mathbf{r}, \mathbf{r}') = \sum_{ij} \Psi_i^*(\mathbf{r}) v_{ij} \Psi_j(\mathbf{r}'). \quad (6)$$

In the system of a spherical QD, $\Psi_i(\mathbf{r})$ should be chosen as $j_l(k_{ln} r) Y_{lm}(\theta, \phi)$ and the indices i and j stand for the abbreviations of the indices $\{l, n, m\}$ and $\{l', n', m'\}$, respectively. Therefore, in SI[37] units, the Coulomb potential energy between electrons and holes is expressed as $v(\mathbf{r}, \mathbf{r}') = Q^2/(4\pi\epsilon_0 |\mathbf{r} - \mathbf{r}'|)$, where Q denotes the charge quantity of carriers and ϵ_0 is the permittivity of vacuum. Replacing the factor $(Q^2/4\pi\epsilon_0)$ by the constant A, the potential energy can also be expanded as

$$v(\mathbf{r}, \mathbf{r}') = A \sum_l \left(\frac{r_<^l}{r_>^{l+1}} \right) \frac{4\pi}{2l+1} \sum_{m=-l}^{l} Y_{lm}^*(\theta, \phi) Y_{lm}(\theta', \phi'). \quad (7)$$

One may notice that $v(\mathbf{r}, \mathbf{r}') = v(\mathbf{r}', \mathbf{r})$.

Fortunately, the radial part in Eq. (7) can be expanded by the spherical Bessel functions j_l as

$$\frac{r_<^l}{r_>^{l+1}} = \sum_{nn'} C_{lnn'} j_l(k_{ln} r) j_l(k_{ln'} r'), \quad (8)$$

where the coefficient $C_{lnn'}$ takes the form of

$$C_{lnn'} = \frac{2}{R^3[j_{l+1}(k_{ln}R)]^2}\left\{\frac{2l+1}{k_{ln}^2}\delta_{nn'}\right.$$
$$\left.+\frac{2}{R^3[j_{l+1}(k_{ln'}R)]^2}\frac{R^3}{k_{ln}k_{ln'}}j_{l+1}(k_{ln}R)j_{l+1}(k_{ln'}R)\right\}.$$

(9)

Here, R is the radius of a QD and $\delta_{nn'}$ is the usual Kronecker delta.[31] The details of the derivation are presented in Appendix A. Then, the Coulomb potential energy can be expanded as Eq. (6), and the matrix elements v_{ij} could be expressed in a concise form

$$v_{ln,l'n'} = \delta_{ll'}A\frac{4\pi}{2l+1}C_{lnn'},$$

(10)

which is independent of the quantum number m.

As mentioned before, $\epsilon(\mathbf{r},\mathbf{r}';\omega)$ should be expanded in terms of wave-functions $\Psi_i^*(\mathbf{r})$ and $\Psi_j(\mathbf{r}')$ as Eq. (2), where quantum numbers i and j are the abbreviations of the indices $\{l,n,m\}$ and $\{\bar{l},\bar{n},\bar{m}\}$, respectively. By collecting Eqs. (1), (5), and (6) together, one can obtain the elements of dielectric matrix (DM), $\epsilon_{ij}(\omega)$ in Eq. (2), given by

$$\epsilon_{ln,\bar{l}\bar{n}}(\omega) = \epsilon_s\delta_{l\bar{l}}\left\{\frac{2}{R^3[j_{l+1}(k_{ln}R)]^2}\delta_{n\bar{n}}\right.$$
$$-\frac{A}{\epsilon_s}\sum_{n'}\sum_{l_1n_1}^{occ}\sum_{l_2n_2}^{unocc}C_{lnn'}\frac{2}{R^3[j_{l\bar{n}}(k_{l\bar{n}}R)]^2}\mathcal{J}_{n'n_1n_2}^{ll_1l_2}\mathcal{\bar{J}}_{\bar{n}n_1n_2}^{\bar{l}l_1l_2}$$
$$\left.\times\frac{(2l_1+1)(2l_2+1)}{2l+1}\begin{pmatrix}l_1 & l_2 & l\\0 & 0 & 0\end{pmatrix}^2\mathcal{W}(\omega)_{\substack{l_2,n_2\\l_1,n_1}}\right\},$$

(11)

where

$$\mathcal{J}_{n'n_1n_2}^{ll_1l_2} \equiv \int r''^2dr''j_l(k_{ln'}r'')\Xi_{l_1n_1}(r'')\Xi_{l_2n_2}(r''),\quad (12)$$

and

$$\mathcal{\bar{J}}_{\bar{n}n_1n_2}^{\bar{l}l_1l_2} \equiv \int r'^2dr'j_{\bar{l}}(k_{l\bar{n}}r')\Xi_{l_1n_1}(r')\Xi_{l_2n_2}(r').\quad (13)$$

The notation $\mathcal{W}(\omega)_{\substack{l_2,n_2\\l_1,n_1}}$ represents the terms inside the braces of Eq. (5), and the Wigner $3j$ symbol[38,39] is introduced in Eq. (11). The detailed presentation can be found in AppendixB. We should notice that the elements of DM are independent of the quantum number m. Spherical symmetry possessed by the QD implies the fact that the angular part of the polarization function $P(\mathbf{r},\mathbf{r}';\omega)$ expressed in Eq. (5), as well as the dielectric function $\epsilon(\mathbf{r},\mathbf{r}';\omega)$, depends only on the angle between vectors $\mathbf{r}$ and $\mathbf{r}'$, which can be verified by the addition theorem for spherical harmonics

$$P_l(\cos\gamma) = \frac{4\pi}{2l+1}\sum_{m=-l}^{l}Y_{lm}^*(\theta,\phi)Y_{lm}(\theta',\phi'),$$

where γ indicates the angle between (r,θ,ϕ) and (r',θ',ϕ').

It will be useful for subsequent formulation to define the energy level difference, $\Delta E_{\substack{l_2,n_2\\l_1,n_1}}\equiv E_{l_2n_2}^{unocc}-E_{l_1n_1}^{occ}$. The real part of $\mathcal{W}(\omega)_{\substack{l_2,n_2\\l_1,n_1}}$ can be deduced as

$$\mathrm{Re}\left[\mathcal{W}(\omega)_{\substack{l_2,n_2\\l_1,n_1}}\right] = \frac{2\left(\Delta E_{\substack{l_2,n_2\\l_1,n_1}}\right)}{\hbar^2\omega^2-\left(\Delta E_{\substack{l_2,n_2\\l_1,n_1}}\right)^2}.$$

(14)

According to Eqs. (11) and (14), the real part of the elements in DM takes the block-matrix structure

$$\mathrm{Re}[\epsilon(\omega)]$$
$$=\begin{pmatrix}\begin{matrix}l=0,\mathrm{n}\times\bar{\mathrm{n}}\\ \mathrm{block}\end{matrix} & 0 & 0 & 0\\0 & \begin{matrix}l=1,\mathrm{n}\times\bar{\mathrm{n}}\\ \mathrm{block}\end{matrix} & 0 & 0\\\vdots & \cdots & \ddots & \vdots\\0 & 0 & \cdots & \begin{matrix}l\to\infty,\mathrm{n}\times\bar{\mathrm{n}}\\ \mathrm{block}\end{matrix}\end{pmatrix}.$$

(15)

The elements in the nondiagonal blocks with $l\neq\bar{l}$ in Eq. (15) would be zeros, and the nonvanishing elements would be in the $\mathrm{n}\times\bar{\mathrm{n}}$ diagonal blocks with $l=\bar{l}$. Since the values of n and $\bar{n}$ would be identical, the blocks will assume a square form.

III. SINGLE-PARTICLE-LIKE CHARGE DENSITY EXCITATIONS

This section numerically calculates the SP-like CDEs (Refs. 12 and 16) in charged or electron-doped spherical QDs. We adjust the Fermi level to control the number of occupied states and search for the excitations with angular quantum number l. Finally, this section also discusses the dependence of the excitation energy on the sizes of different material QDs.

Section II above derives DM, which is the ratio of the bare to the renormalized density-density correlation functions. Since the excitation energies are indicated by the pole of the renormalized density-density correlation function,[40,41] these excitation energies can be obtained from the given frequencies ω or the energies $\hbar\omega$ to satisfy[29,42]

$$\det\{\mathrm{Re}[\epsilon(\omega)]\} = 0.$$

(16)

According to the block-matrix structure for $\mathrm{Re}[\epsilon(\omega)]$ in Eq. (15), the determinant of $\mathrm{Re}[\epsilon(\omega)]$ is the product of the determinants of all l blocks. Therefore, one could search for excitation energies in a QD throughout all l blocks.

In the calculations, the Fermi level is adjusted above the conduction-band minimum to control the number of occupied states, and the electron-doped spherical QDs are discussed. When the number of occupied conduction states in Eq. (11) is set below 20, the summation over 80 terms of unoccupied states is sufficient for obtaining accurate results.

TABLE I. The electronic structures for CdS, CdSe, and CdTe QDs with different radius. The index ν denotes the electronic levels, ν =0 corresponds to the ground state, ν=1 corresponds to the first-excited state, etc. The first three columns show the dependence of the quantum numbers l and n, and the degeneracy on ν. The remaining columns display the energy levels in eV for CdS, CdSe, and CdTe QDs with different radius.

ν	0	1	2	3	4	5	6	7	8	9	10	11
l	0	1	2	0	3	1	4	2	5	0	3	6
n	1	1	1	2	1	2	1	2	1	3	2	1
degeneracy	1	3	5	1	7	3	9	5	11	1	7	13
1.5nm CdS	0.84	1.71	2.82	3.35	4.14	5.07	5.68	7.02	7.43	7.54	9.21	9.38
2.3nm CdS	0.36	0.73	1.20	1.43	1.76	2.15	2.42	2.99	3.16	3.21	3.92	3.99
3.1nm CdS	0.20	0.40	0.66	0.78	0.97	1.19	1.33	1.64	1.74	1.77	2.16	2.20
3.9nm CdS	0.12	0.25	0.42	0.50	0.61	0.75	0.84	1.04	1.10	1.12	1.36	1.39
4.7nm CdS	0.09	0.17	0.29	0.34	0.42	0.52	0.58	0.72	0.76	0.77	0.94	0.96
2.3nmCdSe	0.55	1.12	1.84	2.19	2.71	3.31	3.72	4.59	4.86	4.93	6.03	6.14
2.3nmCdTe	0.75	1.53	2.52	3.00	3.71	4.54	5.09	6.29	6.65	6.75	8.25	8.40

To obtain the sufficiently convergent results of the values of zeros of the determinant shown in Eq. (16), it is enough to take the cutoffs of the numbers n and $\bar{n}$, i.e., the dimensions of the blocks, as 12. In addition, this study only examines the QD systems with all degenerate states for each occupied level. For convenience of the subsequent discussion, the calculated electronic levels for QDs based on EMA are listed in Table I and denoted by the index, ν. For example, ν=0 corresponds to the ground conduction state and ν=1 corresponds to the first-excited state, etc. The first three columns of Table I depict the dependence of ν on quantum numbers l and n, and the degeneracy (i.e., $2l+1$), for the first 12 states, which are identical for CdS, CdSe, and CdTe QDs with different radius. The rest of the columns in Table I illustrate the energy levels in eV for QD systems with different compositions and sizes. The level differences in the occupied and unoccupied state energies indicated the single-particle excitation (SPE) energies. These SPEs correspond to the interlevel absorptions, i.e., the excitation energies of electron-hole pairs around the Fermi level.

A. SP-like CDEs for the case of five occupied states (ν=4)

For numerical analysis, begin by investigating the SP-like CDE energies in a CdS QD with R=2.3 nm, whose effective mass is $m_{e,\text{CdS}}$=0.2.[43] For the sake of illustration, consider the case of five occupied states, which contain 17 electrons. Search for excitation energies by going through different l blocks. Figures 1(a)–1(f) present the values of determinants from the l=0 to l=5 block, respectively. For numerical convenience, this study multiplies the matrix elements in Eq. (11) by R^3. Figures 1(a)–1(f) show that the energies corresponding to the poles of the determinants of the l blocks represent the SPE energies. On the other hand, the energies corresponding to zeros of the determinants are the SP-like CDE energies. In Figs. 1(a)–1(f), the points where the x axis intercepts the vertical lines represent the SPE energies, which are labeled by $\Delta E_{l_1,n_1}^{l_2,n_2}$.

Figures 1(a)–1(f) show that the calculated SP-like CDE energy is larger than the calculated SPE energy $\Delta E_{l_1,n_1}^{l_2,n_2}$. In general, a larger value of the relative permittivity ϵ_s leads to a weaker interaction from the valence electrons, and makes the excitation energy closer to the SPE energy. The dependence of the SP-like CDEs on the relative permittivity ϵ_s will be investigated further below.

From Eq. (11) one can verify that the indices l, l_1, and l_2 in the l block and $\Delta E_{l_1,n_1}^{l_2,n_2}$ must obey the selection rules, such as the triangular inequalities, and $l+l_1+l_2$ must be even.[38,39] Referring to Table I, the lowest SPE energy for the ν=4 case is $\Delta E_{3,1}^{1,2}$. This energy can be found in the l=2 and l=4 blocks, as indicated in Figs. 1(c) and 1(e). Both figures show that the energies of the SP-like CDEs around $\Delta E_{3,1}^{1,2}$ with angular quantum numbers l=2 and l=4 differ from each other. Similarly, the SPE energy $\Delta E_{3,1}^{4,1}$ arises in the l=1, l =3, and l=5 blocks, as Figs. 1(b), 1(d), and 1(f) show, respectively. However, the energies of the SP-like CDEs with l=1, l=3, and l=5 close to $\Delta E_{3,1}^{4,1}$ are 0.725, 0.674, and 0.663 eV, respectively. Consequently, these energy differences imply that excitation energies depend on the angular quantum number l even though they are close to the same SPE energy $\Delta E_{l_1,n_1}^{l_2,n_2}$.

It is interesting to note that Fig. 1(a) shows the behavior of the determinant of the l=0 block around some lowest SPEs. The energies of the second and third lowest SPEs are almost the same. The determinant between these two close SPEs assumes a negative value, and both corresponding SP-like CDE energies can be determined with somewhat larger values as shown in Fig. 1(a).

Consequently, the behaviors of the l block determinants are related to the energies of SPEs, $\Delta E_{l_1,n_1}^{l_2,n_2}$, as implied in Eq. (14). After collecting contributions from all combinations between occupied and unoccupied states in Eq. (11), those terms with $\Delta E_{l_1,n_1}^{l_2,n_2}$ close to the given energy $\hbar\omega$ become dominant. Therefore, the SP-like CDEs emerge with energies slightly larger than the SPEs especially in QD systems.[12,13]
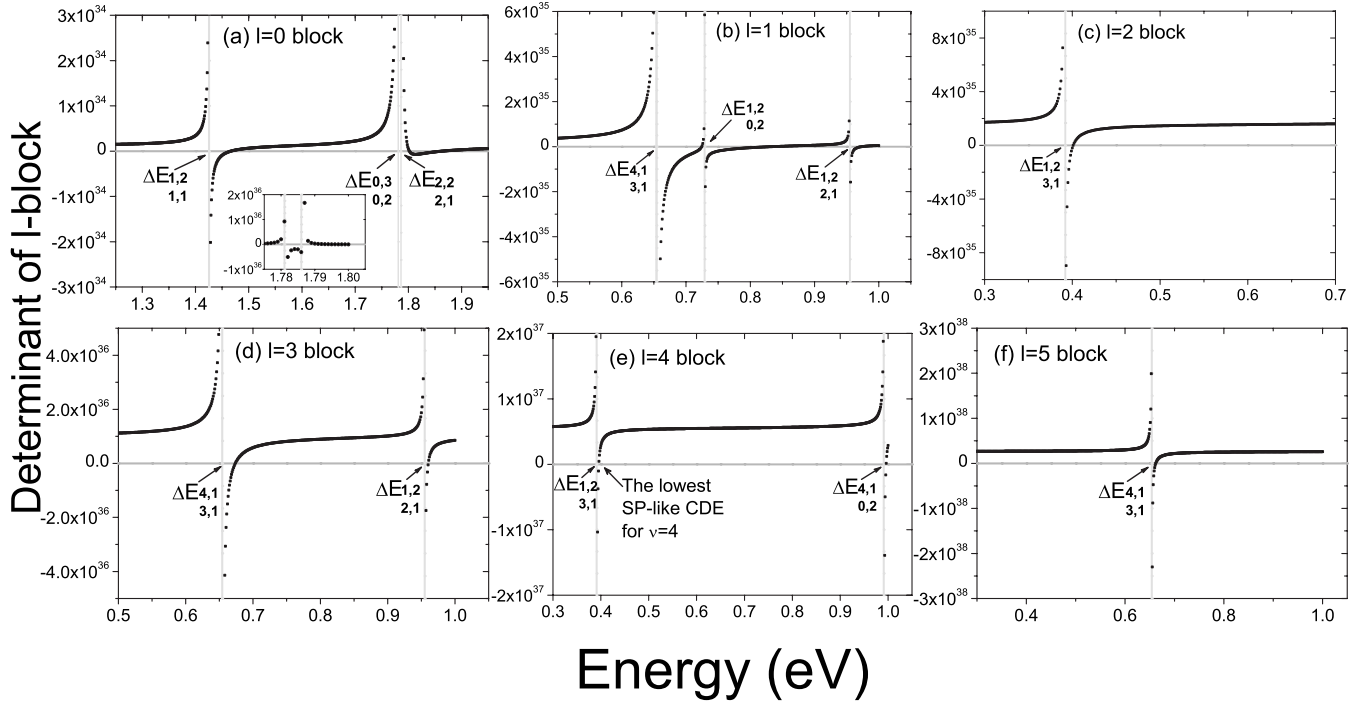
FIG. 1. (a)–(f) Determinants of the $l=0$ to $l=5$ block as a function of the energy in the case of five occupied states. The horizontal lines label the points where the determinants are zero for reference. The vertical lines mark the SPE energies, which are labeled by $\Delta E_{l_1,n_1}^{l_2,n_2}$. The SP-like CDE with the lowest energy for $\nu=4$ is indicated in (e).

Although these SP-like CDEs are known to be weakly collective excitations, they are still observable.[14–16] It is not an easy task to analyze all SP-like CDE energies by going through all l blocks in a QD system. The following study focuses on the behavior of the SP-like CDEs with the lowest energy subject to some given Fermi levels. Moreover, to study the energy for the formation of a SP-like CDE, one can define the energy shift from the SP-like CDE to the SPE as $\bar{\Delta}_{l_1,n_1}^{l_2,n_2}$, and the shift ratio of $\bar{\Delta}_{l_1,n_1}^{l_2,n_2}$ to the SPE energy as $\Gamma_{l_1,n_1}^{l_2,n_2}$. They are given by

$$\bar{\Delta}_{l_1,n_1}^{l_2,n_2} \equiv \mathcal{E}_{l_1,n_1}^{l_2,n_2} - \Delta E_{l_1,n_1}^{l_2,n_2}, \tag{17}$$

and

$$\Gamma_{l_1,n_1}^{l_2,n_2} \equiv \frac{\bar{\Delta}_{l_1,n_1}^{l_2,n_2}}{\Delta E_{l_1,n_1}^{l_2,n_2}}, \tag{18}$$

where $\mathcal{E}_{l_1,n_1}^{l_2,n_2}$ is the calculated SP-like CDE energy with the angular quantum number l and close to the SPE energy

$\Delta E_{l_1,n_1}^{l_2,n_2}$. Here, the energy shift $\bar{\Delta}_{l_1,n_1}^{l_2,n_2}$ is positive, which is consistent with the measurement reported in Refs. [12] and [14]. The shift ratio $\Gamma_{l_1,n_1}^{l_2,n_2}$ can reflect the relative change in energies of the SP-like CDE and the SPE. The dependence of the shift ratio $\Gamma_{l_1,n_1}^{l_2,n_2}$ on the radius and the relative permittivity ϵ_s of QDs will be investigated in the following subsection.

B. SP-like CDEs in charged spherical quantum dots with different sizes and compositions

The energy shift $\bar{\Delta}_{l_1,n_1}^{l_2,n_2}$ and the shift ratio $\Gamma_{l_1,n_1}^{l_2,n_2}$ are calculated in various QDs for some given Fermi levels in this subsection. Table II shows the angular quantum numbers l of the lowest SP-like CDEs for different Fermi levels ν. The lowest SPE energy $\Delta E_{l_1,n_1}^{l_2,n_2}$ in a QD oscillates with the Fermi level ν due to the energy difference between every next levels, and the calculated lowest SP-like CDE energies bear an expected resemblance. Table III shows the calculated SP-like CDEs with the lowest energies $\mathcal{E}_{l_1,n_1}^{l_2,n_2}$, the corresponding SPE energies $\Delta E_{l_1,n_1}^{l_2,n_2}$, the energy shifts $\bar{\Delta}_{l_1,n_1}^{l_2,n_2}$ of the SP-like CDEs

TABLE II. The angular quantum numbers l of the lowest SP-like CDEs for different Fermi levels in a CdS (CdSe or CdTe) QD. The index ν denotes the Fermi level right above the energy level ν.

ν	0	1	2	3	4	5	6	7	8	9	10
l	1	3	2	3	4	5	6	7	5	3	7

TABLE III. When the Fermi level is right above the energy levels $\nu=4$ and $\nu=8$, the lowest SPE energies $\Delta E_{l_1,n_1}^{l_2,n_2}$, the calculated SP-like CDEs with the lowest energies $\mathcal{E}_{l_1,n_1}^{l_2,n_2}$, the energy shifts $\bar{\Delta}_{l_1,n_1}^{l_2,n_2}$, and the shift ratios $\Gamma_{l_1,n_1}^{l_2,n_2}$ for CdS QDs with different radii.

$\nu=4$ (nm)	$\Delta E_{3,1}^{1,2}$ (eV)	$\mathcal{E}_{3,1}^{4}{}_{1,2}$ (eV)	$\bar{\Delta}_{3,1}^{4}{}_{1,2}$ (meV)	$\Gamma_{3,1}^{4}{}_{1,2}$ (%)
1.5	0.921	0.927	6.29	0.68
2.3	0.392	0.396	4.41	1.13
3.1	0.216	0.219	2.94	1.36
3.9	0.136	0.139	2.30	1.69
4.7	0.094	0.096	1.85	1.97
	$\Delta E_{5,1}^{0,3}$ (eV)	$\mathcal{E}_{5,1}^{5}{}_{0,3}$ (eV)	$\bar{\Delta}_{5,1}^{5}{}_{0,3}$ (meV)	$\Gamma_{5,1}^{5}{}_{0,3}$ (%)
$\nu=8$ (nm)				
1.5	0.110	0.113	2.66	2.42
2.3	0.047	0.049	1.75	3.73
3.1	0.026	0.027	1.26	4.91
3.9	0.016	0.017	0.95	5.84
4.7	0.011	0.012	0.76	6.82

with respect to the SPEs, and the shift ratios $\Gamma_{l_1,n_1}^{l_2,n_2}$ for CdS QDs with different radii when the Fermi levels are right above the energy levels $\nu=4$ and $\nu=8$, for example.

Figure 2 depicts the shift ratios $\Gamma_{l_1,n_1}^{l_2,n_2}$ of the lowest SP-like CDEs in CdS QDs with 1.5, 2.3, 3.1, 3.9, and 4.7 nm radius for some given Fermi levels ν. Similarly, the value of $\Gamma_{l_1,n_1}^{l_2,n_2}$ of the lowest SP-like CDE oscillates with the Fermi level ν. Observe that the shift ratio $\Gamma_{l_1,n_1}^{l_2,n_2}$ increases linearly with the
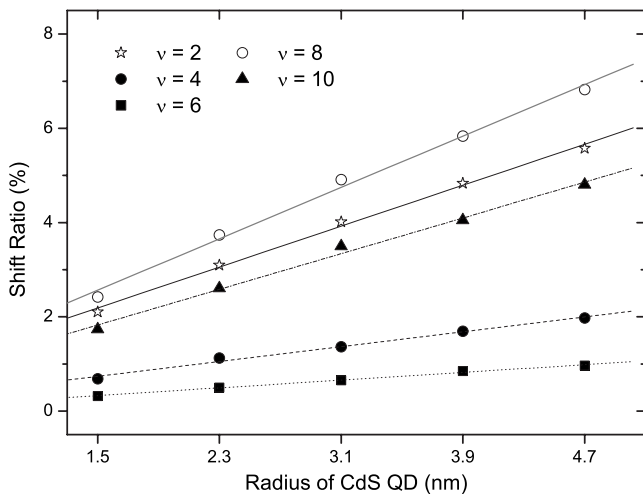

FIG. 2. The shift ratios of the lowest SP-like CDEs versus the radii of CdS QDs for the Fermi levels right above the energy state ν. The index ν is for the ν-th excited state. The data are fitted linearly.
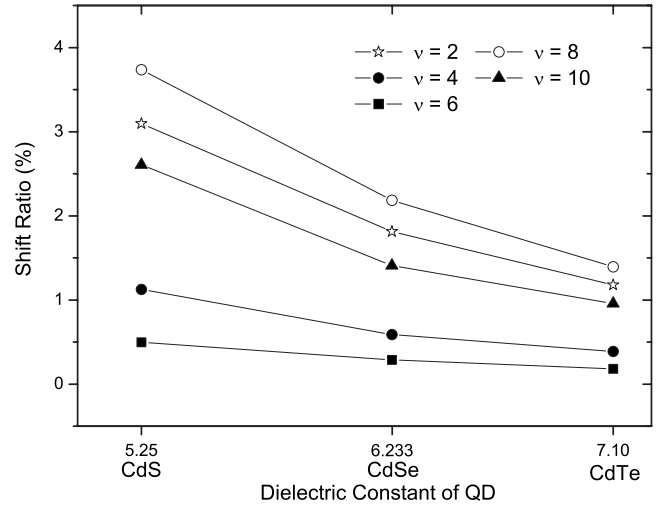

FIG. 3. The shift ratios of the lowest SP-like CDEs versus the dielectric constants (relative permittivities) of CdS ($\epsilon_s=5.25$), CdSe ($\epsilon_s=6.233$), and CdTe ($\epsilon_s=7.1$) QDs with 2.3nm radius for the Fermi levels right above the energy state ν.

radius of a QD for a given ν. The increasing trend of the shift ratio with respect to the radius of a QD could be explained as follows.

From the theoretical viewpoint, quantum-size effects on SP-like CDEs in a semiconductor QD are determined by the competition between the screened Coulomb force and the repulsive confinement force due to the QD boundary.[44–48] In the case of a QD with a smaller radius, the separation between the size-quantization levels of carriers is on the order of $\hbar^2/(m^*R^2)$. This separation energy is larger compared with the energy of the Coulomb interaction, which is on the order of $Q^2/(\epsilon_s R)$. Therefore, the confinement force is dominant in this case. Hence, in our calculations for a given Fermi level ν, the shift ratio is smallest in a QD with 1.5nm radius as Fig. 2 shows. On the other hand, for a QD with a larger radius, one can assume that the center of the mass for a pair of carriers is at a fixed point which is located at a distance from the surface of the QD. For that reason, the influence of the boundary confinement force is found to be weak, and the screened Coulomb force is less severely influenced and dominant in this case. Hence, the shift ratio becomes pronounced with the increase in the radius of the QD as shown in Fig. 2. The larger size will lead to the smaller energy difference $\Delta E_{l_1,n_1}^{l_2,n_2}$, as well as the energy shift $\bar{\Delta}_{l_1,n_1}^{l_2,n_2}$, and the shift ratio $\Gamma_{l_1,n_1}^{l_2,n_2}$ increases with the QD size. In a three-dimensional (3D) bulk system, the limiting case of a 0D spherical QD with a very large radius, the energy level distribution becomes continuous and the energy difference is approximately zero, and the energy shift $\bar{\Delta}_{l_1,n_1}^{l_2,n_2}$ becomes negligible. That implies that the SP-like CDEs will disappear in a 3D bulk system.

Finally, this subsection also examines the dependence of the shift ratio $\Gamma_{l_1,n_1}^{l_2,n_2}$ on the relative permittivity ϵ_s for different semiconductors. Figure 3 depicts the shift ratio of the lowest SP-like CDEs versus the dielectric constants of the

2.3 nm QDs composed by CdS [$\epsilon_s = 5.25$ (Ref. 49)], CdSe [$\epsilon_s = 6.233$ (Ref. 49), $m_{e,\text{CdSe}} = 0.13$ (Ref. 50)], and CdTe [$\epsilon_s = 7.1$, $m_{e,\text{CdTe}} = 0.095$ (Ref. 49)] for some given Fermi levels ν. Observe that the shift ratio qualitatively decreases with the relative permittivity of the semiconductor. As mentioned in Sec. II, a larger ϵ_s leads to a smaller Coulomb potential as Eq. (11) shows, which is tantamount to a weaker interaction due to the screening effect of the valence electrons. However, one can anticipate that in a semiconductor QD with a small ϵ_s, the correlation between the conduction and valence electrons turns into prominent in this system, and the energy shift becomes pronounced.

In addition, both the energy level difference $\Delta E^{l_2,n_2}_{l_1,n_1}$ and the energy shift $\bar{\Delta}^{l}_{\substack{l_2,n_2 \\ l_1,n_1}}$ change with the effective mass as indicated in Eq. (4). Table I tabulates the electronic levels calculated by EMA for the CdSe and CdTe QDs, and the SPE energy can be determined. However, the screening effect should not be affected by different effective masses, and in a hole-carrier QD system will bear a resemblance to the behavior of the SP-like CDE in an electron-carrier QD system.

IV. CONCLUSIONS AND DISCUSSION

In this work, the single-band EMA is adopted to obtain the electron (hole) envelope functions and energy level differences in a spherical semiconductor QD. With the aid of the obtained envelope functions, the RPA-based generalized polarization function of electrons is exploited to derive the dielectric function analytically. This study expands the dielectric function with the basis, $j_l(k_{ln}r)Y_{lm}(\theta,\phi)$, and obtains the dielectric matrix with the block structure. The independence of dielectric matrix elements on the quantum number m is revealed due to spherical symmetry in a spherical QD. By numerically finding zeros of the real parts of the determinants of the dielectric matrix, we determine the SP-like CDEs for the given l quantum numbers. The SP-like CDEs emerge with energies slightly larger than those of the SPEs as observed by the resonant Raman scattering,[14,15] even though these SP-like CDEs might be weakly collective excitations as reported by some groups.[12,13,16] In the case of a charged or electron-doped QD, the Fermi level is adjusted to control the number of occupied conduction states. Then, the relation between the SP-like CDE energy and the size of a QD is investigated. The excitation energy shift with respect to the SPE and the shift ratio are discussed. Efros, Kayanuma, and co-workers[45–48] elaborated the mechanism dictating the screening effect in a confinement system. Similarly, in our calculations for SP-like CDEs in QDs, the size effect bears a resemblance. The competition between the screened Coulomb force and the repulsive confinement force plays a decisive role in the dependence of the shift ratio on the QD size. In particular, in the limit of the infinite QD radius, the calculated SP-like CDE energy goes to zero, and the excitation will disappear. Moreover, the SP-like CDE energies vary with the compositions of QDs. The larger relative permittivity ϵ_s, which is tantamount to a weaker interaction due to the valence electrons, leads to the smaller SP-like CDE energy shift with respect to the SPE.

Experimentally, the SP-like CDEs in QDs can be probed by the resonant Raman scattering (RRS).[12,14] Generally, the RRS technique is a spectroscopic tool to study plasmon energy.[4] In the RRS experiment, external phonons are absorbed at one frequency and one momentum, and emitted at another, creating excitations. The energy and momentum difference between the incident photon and the scattered one is the so-called Stokes shift, revealing the dispersion of the relevant elementary electronic excitation originated in the system. As demonstrated in Ref. 12 and Ref. 16, additional SP-like SDEs can be observed, which could be calculated by including the electron spin degree of freedom in our formulism in the future work.

APPENDIX A: THE COEFFICIENT OF COULOMB POTENTIAL EXPANDED WITH j_l BASIS

In this appendix, the coefficient $C_{lnn'}$ in Eq. (8) is derived. According to the orthonormality of the basis functions labeled by the roots of the spherical Bessel function with a given integral order l, any well-behaved but otherwise arbitrary function $f(r)$ may be expanded in a spherical Bessel series[31] $f(r) = \sum_{n=1}^{\infty} C'_{ln} j_l(\alpha_{ln} r/R)$, where α_{ln} is the nth zero of j_l; that is, $j_l(\alpha_{ln}) = 0$. The coefficient C'_{ln} can be determined by the orthonormality

$$C'_{ln} = \frac{2}{R^3[j_{l+1}(\alpha_{ln})]^2} \int_0^R f(r) j_l\left(\alpha_{ln}\frac{r}{R}\right) r^2 dr.$$

Furthermore, $j_l(k_{ln}r)$ is the radial part of an envelope function in a QD and $j_l(k_{ln}R) = 0$ because of the boundary-condition $\psi(\mathbf{r})|_{r=R} = 0$. We can choose $\alpha_{ln} = k_{ln}R$ to expand the radial part of the Coulomb potential in Eq. (7). The determination of the coefficient $C_{lnn'}$ in Eq. (8) will be facilitated by expanding $(r_<^l)/(r_>^{l+1})$ in terms of $j_l(k_{ln}r)$ such as

$$\frac{r_<^l}{r_>^{l+1}} = \sum_n \bar{C}_{ln} j_l(k_{ln}r).$$

The employment of the orthonormality relations yields

$$\bar{C}_{ln} = \frac{2}{R^3[j_{l+1}(k_{ln}R)]^2}\left[\frac{2l+1}{k_{ln}^2} j_l(k_{ln}r') - \frac{r'^l R^{1-l}}{k_{ln}} j_{l-1}(k_{ln}R)\right]$$

$$= \frac{2}{R^3[j_{l+1}(k_{ln}R)]^2}\left[\frac{2l+1}{k_{ln}^2} j_l(k_{ln}r') + \frac{r'^l R^{1-l}}{k_{ln}} j_{l+1}(k_{ln}R)\right].$$

Then we expand the r'-dependent by the spherical Bessel-functions $j_l(k_{ln'}r')$ and again make use of the orthonormality. Finally, we end up with the expression for $C_{lnn'}$

$$C_{lnn'} = \frac{2}{R^3[j_{l+1}(k_{ln}R)]^2} \left\{ \frac{2l+1}{k_{ln}^2} \delta_{nn'} \right.$$
$$\left. - \frac{2}{R^3[j_{l+1}(k_{ln'}R)]^2} \frac{R^3}{k_{ln}k_{ln'}} j_{l-1}(k_{ln}R)j_{l+1}(k_{ln'}R) \right\}$$
$$= \frac{2}{R^3[j_{l+1}(k_{ln}R)]^2} \left\{ \frac{2l+1}{k_{ln}^2} \delta_{nn'} \right.$$
$$\left. + \frac{2}{R^3[j_{l+1}(k_{ln'}R)]^2} \frac{R^3}{k_{ln}k_{ln'}} j_{l+1}(k_{ln}R)j_{l+1}(k_{ln'}R) \right\}.$$

Both expressions are equivalent and the second one is more suitable for our calculations.

APPENDIX B: THE INTEGRAL TO CALCULATE DIELECTRIC FUNCTION

In this appendix, we deal with the integral in Eq. (1) and expand the dielectric function $\epsilon(r,r';\omega)$ in terms of $\Psi_i^*(r)$ and $\Psi_j(r')$. The Wigner $3j$ symbol[38,39] is introduced in this appendix and some properties of the $3j$ symbol are employed to simplify the expression to justify spherical symmetry in a QD.

To begin with, the integral in Eq. (1) can be rewritten as

$$\int d^3r'' v(r,r'') P(r'',r';\omega)$$

$$= \int d^3r'' A \sum_{lmnn'} \sum_{l_1m_1n_1}^{\text{occ}} \sum_{l_2m_2n_2}^{\text{unocc}} C_{lnn'} j_l(k_{ln}r) j_l(k_{ln'}r'')$$

$$\times \frac{4\pi}{2l+1} Y_{lm}^*(\theta,\phi) Y_{lm}(\theta'',\phi'')$$

$$\times \Xi_{l_1n_1}(r'') \Xi_{l_2n_2}(r'') \Xi_{l_2n_2}(r') \Xi_{l_1n_1}(r')$$

$$\times Y_{l_1m_1}^*(\theta'',\phi'') Y_{l_2m_2}(\theta'',\phi'') Y_{l_2m_2}^*(\theta',\phi')$$

$$\times Y_{l_1m_1}(\theta',\phi') \mathcal{W}(\omega)_{\substack{l_2,n_2 \\ l_1,n_1}}, \qquad (B1)$$

where $\mathcal{W}(\omega)_{\substack{l_2,n_2 \\ l_1,n_1}}$ represents the terms inside the braces of Eq. (5). In Eq. (B1) both integrals of radial and angular parts can be carried out, and the radial part integral is given as

$$\int r''^2 dr'' j_l(k_{ln'}r'') \Xi_{l_1n_1}(r'') \Xi_{l_2n_2}(r'') \equiv \mathcal{J}_{n'n_1n_2}^{ll_1l_2}, \quad (B2)$$

where the function $\mathcal{J}_{n'n_1n_2}^{ll_1l_2}$ is introduced. In this work, the integral in Eq. (B2) is evaluated numerically. On the other hand, the angular part integral is known to be

$$\int d\Omega'' Y_{lm}(\theta'',\phi'') Y_{l_1m_1}^*(\theta'',\phi'') Y_{l_2m_2}(\theta'',\phi'')$$

$$\equiv \langle Y_{l_1m_1} | Y_{lm} | Y_{l_2m_2} \rangle$$

$$= (-1)^{m_1} \sqrt{\frac{(2l+1)(2l_1+1)(2l_2+1)}{4\pi}}$$

$$\times \begin{pmatrix} l_1 & l & l_2 \\ 0 & 0 & 0 \end{pmatrix} \begin{pmatrix} l_1 & l & l_2 \\ -m_1 & m & m_2 \end{pmatrix}, \qquad (B3)$$

where $\begin{pmatrix} l_a & l_b & l_c \\ m_a & m_b & m_c \end{pmatrix}$ is the Wigner $3j$ symbol.[38,39] Then, Eq. (B1) can be simplified to

$$\int d^3r'' v(r,r'') P(r'',r';\omega)$$

$$= A \sum_{lmnn'} \sum_{l_1m_1n_1}^{\text{occ}} \sum_{l_2m_2n_2}^{\text{unocc}} C_{lnn'} \frac{4\pi}{2l+1} j_l(k_{ln}r) Y_{lm}^*(\theta,\phi)$$

$$\times \Xi_{l_2n_2}(r') \Xi_{l_1n_1}(r') \mathcal{J}_{n'n_1n_2}^{ll_1l_2} \langle Y_{l_1m_1} | Y_{lm} | Y_{l_2m_2} \rangle$$

$$\times Y_{l_2m_2}^*(\theta',\phi') Y_{l_1m_1}(\theta',\phi') \mathcal{W}(\omega)_{\substack{l_2,n_2 \\ l_1,n_1}}. \qquad (B4)$$

Similarly, we can expand the r'-dependence parts in Eq. (B4) by $\Psi_j(r') = j_{\bar{l}}(k_{\bar{l}\bar{n}}r') Y_{\bar{l}\bar{m}}(\theta',\phi')$, such as

$$\Xi_{l_2n_2}(r') \Xi_{l_1n_1}(r') = \sum_{\bar{l}\bar{n}} \widetilde{C}_{\bar{n}n_1n_2}^{\bar{l}l_1l_2} j_{\bar{l}}(k_{\bar{l}\bar{n}}r'), \qquad (B5)$$

and

$$Y_{l_2m_2}^*(\theta',\phi') Y_{l_1m_1}(\theta',\phi') = \sum_{\bar{l}\bar{m}} \widetilde{C'}_{\bar{m}m_1m_2}^{\bar{l}l_1l_2} Y_{\bar{l}\bar{m}}(\theta',\phi'). \qquad (B6)$$

To determine the coefficients, $\widetilde{C}_{\bar{n}n_1n_2}^{\bar{l}l_1l_2}$ and $\widetilde{C'}_{\bar{m}m_1m_2}^{\bar{l}l_1l_2}$, in Eqs. (B5) and (B6), we would deal with both integrals

$$\widetilde{C}_{\bar{n}n_1n_2}^{\bar{l}l_1l_2} = \frac{2}{R^3[j_{\bar{l}+1}(k_{\bar{l}\bar{n}}R)]^2} \int r'^2 dr' j_{\bar{l}}(k_{\bar{l}\bar{n}}r') \Xi_{l_2n_2}(r') \Xi_{l_1n_1}(r')$$

$$= \frac{2}{R^3[j_{\bar{l}+1}(k_{\bar{l}\bar{n}}R)]^2} \mathcal{J}_{\bar{n}n_1n_2}^{\bar{l}l_1l_2}, \qquad (B7)$$

and

$$\widetilde{C'}_{\bar{m}m_1m_2}^{\bar{l}l_1l_2} = \int d\Omega' Y_{\bar{l}\bar{m}}^*(\theta',\phi') Y_{l_2m_2}^*(\theta',\phi') Y_{l_1m_1}(\theta',\phi')$$

$$\equiv [\langle Y_{l_1m_1} | Y_{\bar{l}\bar{m}} | Y_{l_2m_2} \rangle]^*$$

$$= (-1)^{\bar{m}+m_2} \sqrt{\frac{(2\bar{l}+1)(2l_1+1)(2l_2+1)}{4\pi}} \begin{pmatrix} l_1 & \bar{l} & l_2 \\ 0 & 0 & 0 \end{pmatrix}$$

$$\times \begin{pmatrix} l_1 & \bar{l} & l_2 \\ m_1 & -\bar{m} & -m_2 \end{pmatrix}. \qquad (B8)$$

By collecting Eqs. (B4), (B7), and (B8) together, we obtain

$$\int d^3 r'' v(\boldsymbol{r},\boldsymbol{r}'') P(\boldsymbol{r}'',\boldsymbol{r}';\omega)$$

$$= A \sum_{\substack{lmnn' \\ \bar{l}\bar{m}\bar{n}}} \sum_{l_1 m_1 n_1}^{\text{occ}} \sum_{l_2 m_2 n_2}^{\text{unocc}} C_{lnn'}$$

$$\times \frac{4\pi}{2l+1} j_l(k_{ln}r) Y_{lm}^*(\theta,\phi) j_{\bar{l}}(k_{\bar{l}\bar{n}}r') Y_{\bar{l}\bar{m}}(\theta',\phi')$$

$$\times \mathcal{J}_{n' n_1 n_2}^{l l_1 l_2} \langle Y_{l_1 m_1} | Y_{lm} | Y_{l_2 m_2} \rangle \frac{2}{R^3 [j_{\bar{l}+1}(k_{\bar{l}\bar{n}}R)]^2} \mathcal{J}_{\bar{n} n_1 n_2}^{\bar{l} l_1 l_2}$$

$$\times [\langle Y_{l_1 m_1} | Y_{\bar{l}\bar{m}} | Y_{l_2 m_2} \rangle]^* \mathcal{W}(\omega)_{\substack{l_2, n_2 \\ l_1, n_1}}. \tag{B9}$$

The simplification of Eq. (B9) can be achieved by using the identity

$$\sum_{m_1 m_2} \langle Y_{l_1 m_1} | Y_{lm} | Y_{l_2 m_2} \rangle [\langle Y_{l_1 m_1} | Y_{\bar{l}\bar{m}} | Y_{l_2 m_2} \rangle]^*$$

$$= \sum_{m_1 m_2} (-1)^{\bar{m}+m_2+m_1} \frac{(2l_1+1)(2l_2+1)}{4\pi}$$

$$\times \sqrt{(2l+1)(2\bar{l}+1)} \begin{pmatrix} l_1 & l_2 & l \\ 0 & 0 & 0 \end{pmatrix} \begin{pmatrix} l_1 & l_2 & l \\ -m_1 & m_2 & m \end{pmatrix}$$

$$\times \begin{pmatrix} l_1 & l_2 & \bar{l} \\ 0 & 0 & 0 \end{pmatrix} \begin{pmatrix} l_1 & l_2 & \bar{l} \\ m_1 & -m_2 & -\bar{m} \end{pmatrix}, \tag{B10}$$

where the relation

$$\begin{pmatrix} l_a & l_b & l_c \\ m_a & m_b & m_c \end{pmatrix} = (-1)^{l_a+l_b+l_c} \begin{pmatrix} l_a & l_c & l_b \\ m_a & m_c & m_b \end{pmatrix}$$

is applied and l_1+l_2+l (or $l_1+l_2+\bar{l}$) should be even and $m+m_2-m_1$ (or $m_1-m_2-\bar{m}$) should be zero.[38,39] We can ex-

ploit the property of the $3j$ symbols in Eq. (B10) to obtain

$$\sum_{m_1 m_2} (-1)^{\bar{m}+m_2-m_1} \begin{pmatrix} l_1 & l_2 & l \\ -m_1 & m_2 & m \end{pmatrix} \begin{pmatrix} l_1 & l_2 & \bar{l} \\ -m_1 & m_2 & \bar{m} \end{pmatrix} = \frac{\delta_{l\bar{l}}\delta_{m\bar{m}}}{2l+1}.$$

Therefore, Eq. (B10) is simplified to

$$\sum_{m_1 m_2} \langle Y_{l_1 m_1} | Y_{lm} | Y_{l_2 m_2} \rangle [\langle Y_{l_1 m_1} | Y_{\bar{l}\bar{m}} | Y_{l_2 m_2} \rangle]^*$$

$$= \frac{(2l_1+1)(2l_2+1)}{4\pi} \begin{pmatrix} l_1 & l_2 & l \\ 0 & 0 & 0 \end{pmatrix}^2 \delta_{l\bar{l}}\delta_{m\bar{m}},$$

and we acquire

$$\int d^3 r'' v(\boldsymbol{r},\boldsymbol{r}'') P(\boldsymbol{r}'',\boldsymbol{r}';\omega)$$

$$= A \sum_{lmnn'\bar{n}} \sum_{l_1 n_1}^{\text{occ}} \sum_{l_2 n_2}^{\text{unocc}} C_{lnn'} j_l(k_{ln}r) Y_{lm}^*(\theta,\phi) j_l(k_{l\bar{n}}r') Y_{lm}(\theta',\phi')$$

$$\times \frac{2}{R^3 [j_{l+1}(k_{l\bar{n}}R)]^2} \mathcal{J}_{n' n_1 n_2}^{l l_1 l_2} \mathcal{J}_{\bar{n} n_1 n_2}^{\bar{l} l_1 l_2}$$

$$\times \frac{(2l_1+1)(2l_2+1)}{2l+1} \begin{pmatrix} l_1 & l_2 & l \\ 0 & 0 & 0 \end{pmatrix}^2 \mathcal{W}(\omega)_{\substack{l_2, n_2 \\ l_1, n_1}}. \tag{B11}$$

In the calculation, the Dirac delta function is also expanded in terms of the spherical Bessel functions and spherical harmonics

$$\delta(\boldsymbol{r}-\boldsymbol{r}') = \sum_{lmn} \frac{2}{R^3 [j_{l+1}(k_{ln}R)]^2} j_l(k_{ln}r) j_l(k_{l\bar{n}}r')$$

$$\times Y_{lm}^*(\theta,\phi) Y_{lm}(\theta',\phi') \delta_{n\bar{n}}.$$

Consequently, the elements of DM can be expressed as Eq. (11), and are independent of the quantum number m.

---

*Corresponding author; tyan@phy.ccu.edu.tw

[1] S. Das Sarma and W.-y. Lai, Phys. Rev. B **32**, 1401 (1985).

[2] R. Daling, W. van Haeringen, and B. Farid, Phys. Rev. B **44**, 2952 (1991).

[3] S. Das Sarma and D.-W. Wang, Phys. Rev. Lett. **83**, 816 (1999).

[4] D.-W. Wang and S. Das Sarma, Phys. Rev. B **65**, 125322 (2002).

[5] E. H. Hwang and S. Das Sarma, Phys. Rev. B **75**, 205418 (2007).

[6] C. Delerue, G. Allan, and Y. M. Niquet, Phys. Rev. B **72**, 195316 (2005).

[7] M. S. Kushwaha and H. Sakaki, Phys. Rev. B **69**, 155331 (2004).

[8] M. S. Kushwaha, Phys. Rev. B **77**, 241305(R) (2008).

[9] S. S. Sokolov and N. Studart, Phys. Rev. B **57**, R704 (1998).

[10] N. J. M. Horing and L. Y. Chen, Phys. Rev. B **74**, 195336 (2006).

[11] T.-T. Kang, R. Q. Zhang, W. G. Hu, G. W. Cong, F. A. Zhao, X. X. Han, S. Y. Yang, X. L. Liu, Q. S. Zhu, and Z. G. Wang, Phys. Rev. B **76**, 075345 (2007).

[12] C. Steinebach, C. Schüller, and D. Heitmann, Phys. Rev. B **59**, 10240 (1999).

[13] C. Steinebach, C. Schüller, and D. Heitmann, Phys. Rev. B **61**, 15600 (2000).

[14] C. Steinebach, C. Schüller, E. Ulrichs, Ch. Heyn, and D. Heitmann, Phys. Status Solidi B **224**, 97 (2001).

[15] C. Schüller, C. Steinebach, and D. Heitmann, Solid State Commun. **119**, 323 (2001).

[16] C. Schüller, *Inelastic Light Scattering of Semiconductor Nanostructures* (Springer, Berlin, Heidelberg, 2006).

[17] G. D. Mahan, *Many-Particle Physics*, 3rd ed. (Kluwer Academic, New York, 2000).

[18] D. Bohm and D. Pines, Phys. Rev. **82**, 625 (1951).

[19] D. Pines and D. Bohm, Phys. Rev. **85**, 338 (1952).

[20] D. K. Ferry and S. M. Goodnick, *Transport in Nanostrucutres* (Cambridge University Press, Cambridge, 1997).

[21] H. Haug and S. W. Koch, *Quantum Theory of the Optical and*

Electronic Properties of Semiconductors, 4th ed. (World Scientific, Singapore, 2004).

[22] J. W. Haus, H. S. Zhou, I. Honma, and H. Komiyama, Phys. Rev. B **47**, 1359 (1993).

[23] D. Schooss, A. Mews, A. Eychmüller, and H. Weller, Phys. Rev. B **49**, 17072 (1994).

[24] C. L. Weng, I. Chuen Chen, and Y. C. Tsai, Phys. Rev. B **76**, 195313 (2007).

[25] M. Gell-Mann and K. A. Brueckner, Phys. Rev. **106**, 364 (1957).

[26] H. Ehrenreich and M. H. Cohen, Phys. Rev. **115**, 786 (1959).

[27] B. Farid, G. E. Engel, R. Daling, and W. van Haeringen, Phys. Rev. B **44**, 13349 (1991).

[28] G. E. Engel and B. Farid, Phys. Rev. B **46**, 15812 (1992).

[29] W. G. Aulbur, L. Jönsson, and J. W. Wilkins, *Solid State Physics*, edited by H. Ehrenreich and F. Spaepen (Academic, New York, 2000), Vol. 54.

[30] A. L. Fetter and J. D. Walecka, *Quantum Theory of Many-Particle Systems* (McGraw-Hill, New York, 1971).

[31] G. B. Arfken and H. J. Weber, *Mathematical Methods For Physicists*, 6th ed. (Academic, London, 2005).

[32] D. K. Ferry, *Semiconductors* (Macmillan, New York, 1991).

[33] G. Grosso and G. P. Parravicini, *Solid State Physics* (Academic, San Diego, 2000).

[34] L. Hedin, Phys. Rev. **139**, A796 (1965).

[35] L. Hedin and S. Lundqvist, in *Solid State Physics*, edited by H. Ehrenreich, F. Seitz, and D. Turnbull (Academic, New York, 1969), Vol. 23.

[36] F. Aryasetiawan and O. Gunnarsson, Rep. Prog. Phys. **61**, 237 (1998).

[37] J. D. Jackson, *Classical Electrodynamics* (3rd. Edition) (John Wiley & Sons, New York, 1988).

[38] R. N. Zare, *Angular Momentum* (John Wiley & Sons, New York, 1988).

[39] D. M. Brink and G. R. Satchler, *Angular Momentum*, 3rd Ed. (Oxford, New York 1993).

[40] Q. P. Li and S. Das Sarma, Phys. Rev. B **43**, 11768 (1991).

[41] M. S. Kushwaha, Surf. Sci. Rep. **41**, 1 (2001).

[42] L. P. Kadanoff and G. Baym, *Quantum Statistical Mechanics* (Addison-Wesley, New York, 1989).

[43] *Zahlenwerte und Funktionen aus Naturwissenschaften und Technik*, Landolt-Börnstein, New Series, Group III, Vol. 3–17b (Springer, New York, 1982).

[44] D. C. Mattis and G. Beni, Phys. Rev. B **18**, 3816 (1978).

[45] A. L. Efros and A. L. Efros, Sov. Phys. Semicond. **16**, 772 (1982).

[46] Y. Kayanuma, Phys. Rev. B **38**, 9797 (1988).

[47] T. Uozumi and Y. Kayanuma, Phys. Rev. B **65**, 165318 (2002).

[48] G. T. Einevoll, Phys. Rev. B **45**, 3410 (1992).

[49] O. Madelung, *Semiconductors: Data Handbook*, 3rd ed. (Springer, Berlin, Heidelberg, 2004).

[50] R. G. Wheeler and J. O. Dimmock, Phys. Rev. **125**, 1805 (1962).